# Microstructure and magnetic domain structure of boron-enriched $Nd_2(FeCo)_{14}B$ melt-spun ribbons

B. Lu[a],*, M.Q. Huang[a], Q. Chen[b], B.M. Ma[b], D.E. Laughlin[a]

[a]*Department of Materials Science and Engineering, Carnegie Mellon University, 232 Roberts Engineering Hall, Pittsburgh, PA 15213-3890, USA*
[b]*Rhodia Inc., Rare Earths and Gallium, CN 7500, Cranbury, NJ 08512, USA*

## Abstract

Heat treated melt-spun ribbons of $(Nd_{0.95}La_{0.05})_{9.5}Fe_{bal}Co_5Nb_2B_{10.5}$ have been studied systematically by superconducting quantum interference device (SQUID) magnetometry, conventional transmission electron microscopy (CTEM) and Lorentz transmission electron microscopy (LTEM). The sample's microstructure grew from an amorphous state through a partially crystallized state at 650°C, and finally to a fully crystallized state at 750°C. Excessive grain growth producing grains from 38 to 68 nm in diameter was observed when the ribbon was annealed at 850°C. Soft magnetic phases such as $Fe_3B$ and $\alpha$-Fe precipitated at the grain boundaries. These intergranular phases are exchange coupled with the hard phase causing a decrease of $H_c$. Exchange-coupling dominant and dipolar-coupling dominant regions co-exist inside the sample. In the latter regions, snake-shaped interactive domains are frequently observed. © 1999 Elsevier Science B.V. All rights reserved.

*Keywords:* Melt spinning; Magnetic properties; Microstructure; Magnetic domain

## 1. Introduction

Melt-spinning is one of the major commercialized processing routes for the production of NdFeB-based permanent magnets [1]. The microstructure and magnetic properties of the products can be manipulated during the process and subsequent annealing [2–5]. Under carefully controlled conditions, the crystallite size in the isotropic melt-spun ribbon can be limited to the nanocrystalline range (grain size < 100 nm) [6], where each grain is thought to be a single magnetic domain, i.e., domain walls occur predominantly at grain boundaries. As a result, the coercivity of the material will depend strongly on the microstructure of the composites, due to the domain wall nucleation mechanism of the demagnetization process [7–10]. On the other hand, the intergranular magnetic coupling becomes more pronounced when the grain size decreases. In this case, short-range exchange coupling as well as long-range dipolar coupling between the grains will play important roles in the demagnetizing process [11]. Moreover, due to the effect of magnetic coupling the remanence is enhanced. A further improvement can be achieved by adding

---

*Corresponding author. Tel.: + 1-412-268-4034; fax: + 1-412-268-6978.

*E-mail address:* binlu@andrew.cmu.edu (B. Lu)

a soft ferromagnetic phase with a larger $M_s$ (e.g., $\alpha$-Fe, $Fe_3B$) provided that the soft phase is exchange coupled to the hard phase [12–14].

In the present work, the magnetic properties of annealed boron-enriched $Nd_2(FeCo)_{14}B$ melt-spun samples were studied using a superconducting quantum interference device (SQUID) magnetometer. The microstructure, grain size distribution, and intergranular phase were studied with conventional transmission electron microscopy (CTEM). The magnetic domain structure and intergranular magnetic coupling were studied with Lorentz transmission electron microscopy (LTEM). The purpose of this research is to systematically explore the influence of annealing on the microstructure of boron-enriched $Nd_2(FeCo)_{14}B$ melt-spun ribbons, whose magnetic properties are expected to be optimized.

## 2. Experimental

Thermally demagnetized melt-spun samples with the composition of $(Nd_{0.95}La_{0.05})_{9.5}Fe_{bal}$-$Co_5Nb_2B_{10.5}$ were prepared and vacuum annealed (20 mTorr) for 10 min at 650°C (sample A), 700°C (sample B), 750°C (sample C), 850°C (sample D), respectively. The details of the above processes were reported previously [5,15]. The magnetic properties were investigated by a quantum design SQUID magnetometer with a maximum applied field of 50 kOe. The microstructure and crystallinity of the as-spun and thermally-treated ribbons were studied by electron diffraction and diffraction contrast imaging using a Phillip-420 transmission electron microscope (TEM). The magnetic domain structure of sample B, with the optimized magnetic properties, was studied by the Lorentz imaging technique [16] using a JEM-4000 TEM with a Gatan image filter (GIF). Since the ribbons are brittle and of 20 μm thickness, the specimens for TEM observation were prepared directly by ion milling on a cold stage of a GATAN 600 ion miller, followed by ion polishing for less than 5 min at room temperature with a Gatan 691 precision ion polishing system. The ion guns of both machines polished only on the free surface of the ribbons so that TEM observation could be performed on the side opposite the melt-spinning wheel. The TEM for LTEM observation was operated with its objective lens shut off so that there was only a negligible residual field at the position of specimen.

## 3. Microstructure and magnetic properties

Many regions of each single specimen have been observed and recorded by TEM. The result confirms that the microstructures of the samples are very uniform. The bright field image of the as-spun sample (Fig. 1) shows a homogeneous material with no crystalline grains. Also, there is no trace of crystalline reflections in the inset electron diffraction pattern (EDP). These factors indicate that the as-spun sample is fully amorphous.

Fig. 2a is a dark field image of sample A (annealed for 10 min at 650°C) displaying crystalline grains of $Nd_2(FeCo)_{14}B$ embedded in an amorphous matrix. This is consistent with the inset EDP, which shows both $Nd_2(FeCo)_{14}B$ diffraction rings and a diffuse amorphous ring. The image in Fig. 2b shows the lattice fringes of the $Nd_2(FeCo)_{14}B$ phase and the amorphous background. The average grain size is about 40 nm. The small grain with clear 2D fringes (Fig. 2b, black arrow) is a $Nd_2(FeCo)_{14}B$ nucleus in its initial growing stage.
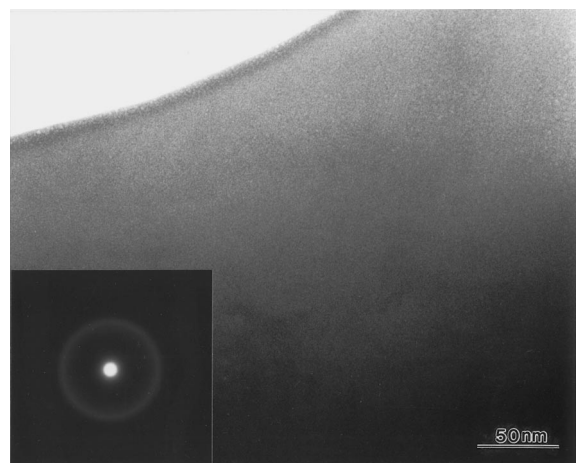


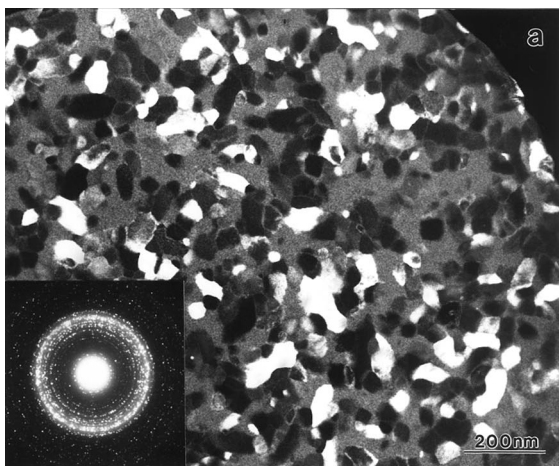Fig. 1. Transmission electron microscopy (TEM) image and electron diffraction pattern (EDP) of as-spun sample.

Fig. 2. (a) TEM image and EDP of 650°C sample, (b) TEM image of higher magnification showing 2D lattice fringes of a small $Nd_2(FeCo)_{14}B$ grain.



Fig. 3. (a) TEM image and EDP of 700°C sample, (b) TEM image of higher magnification.

The images in Fig. 3a and Fig. 3b show well-defined grains of sample B (annealed for 10 min at 700°C) with various facets. The grain size is almost the same as that of sample A. However, the amorphous matrix disappears. The EDP in Fig. 3a exhibits a set of diffraction rings of the specimen. The number of the diffraction rings is greater than that of the EDP in Fig. 2a. This result suggests that either new phases have precipitated or that the $Nd_2(FeCo)_{14}B$ grain has gained a better crystallinity.

Fig. 4a shows that some observable small precipitates start to appear in sample C (annealed for 10 min at 750°C) at the grain boundaries. The small
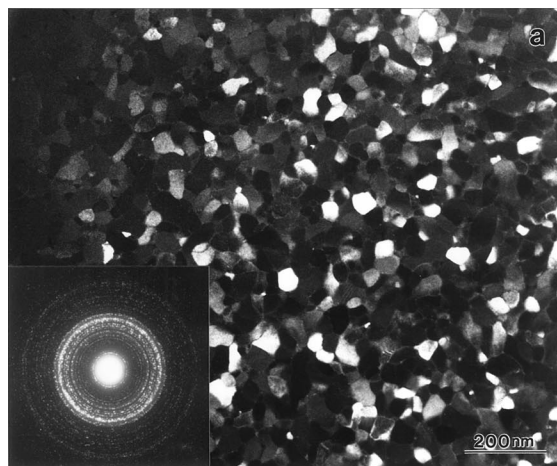
grains are seen more clearly in Fig. 4b as intergranular phases (black arrows). The grain size of the main phase is nearly the same as that found in samples A and B. The average size of the precipitates is less than 5 nm, which is too small to be studied by the micro-diffraction method. Considering that sample C is magnetically softer than sample B (see the hysteresis loops in Fig. 7) and that the ribbons are boron-enriched, these precipitates are most probably grains of $\alpha$-Fe, $Fe_3B$, or other borides.

Fig. 5a shows the grains of both the main phase and intergranular phases are larger in sample
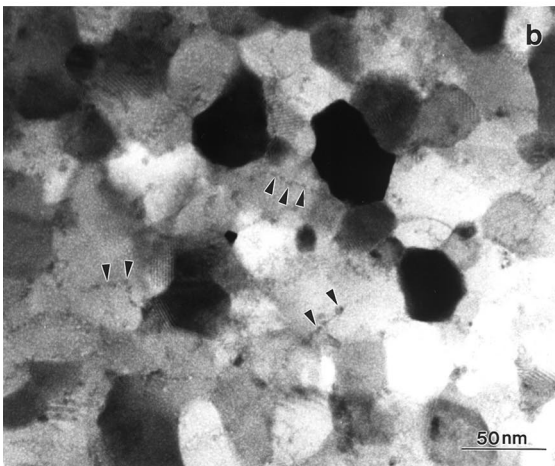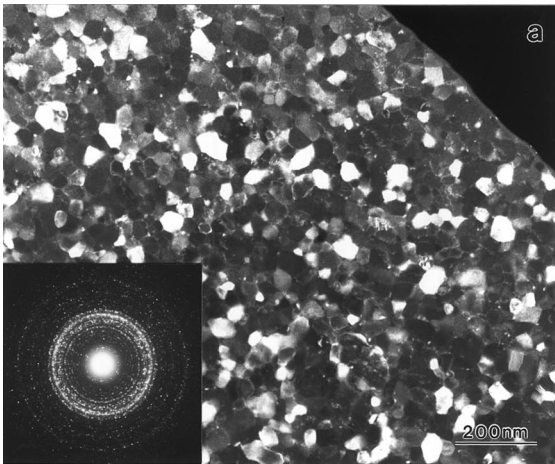
Fig. 4. (a) TEM image and EDP of 750°C sample, (b) TEM image of higher magnification showing small intergranular phases.
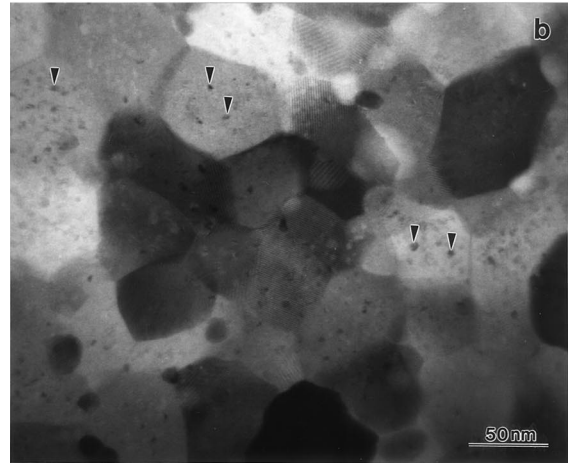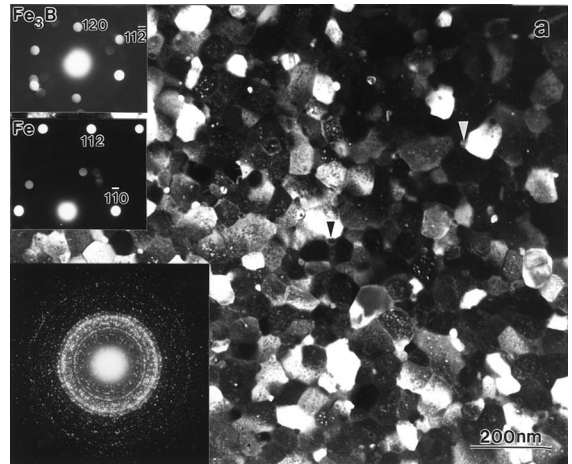


Fig. 5. (a) TEM image and EDP of 850°C sample, (b) TEM image of higher magnification showing the larger intergranular phases and some unidentified small particles everywhere.

D (annealed for 10 min at 850°C). A third type of grain can be observed in Fig. 5b indicated by the arrows. Due to the small grain size of these grains, they have not been characterized so far by either electron diffraction or elemental analysis. The average grain size is about 70 nm for the main phase, and 10 nm for the larger precipitates, on which micro-diffraction was carried out. The top-left insets are the micro-diffraction patterns of $Fe_3B$ and $\alpha$-Fe precipitates, indicated by a white arrow and a black arrow in Fig. 5a, respectively. The fact that some of the larger precipitates are grains of $Fe_3B$ and $\alpha$-Fe suggests that some of the small precipi-

tates in sample C are also the soft magnetic phases, and that they grew larger in sample D.

The grain size distributions of the four annealed samples are plotted in Fig. 6a–Fig. 6d. The histograms are based on data from more than 400 grains in the images of Fig. 2a, Fig. 3a, Fig. 4a and Fig. 5a, respectively. The grain size is calculated as an average value of long axis and short axis of each grain. Fig. 6a shows a nearly symmetrical and wide distribution of grain size from 9 to 100 nm with its average value at 38 nm. Fig. 6b shows a non-symmetric distribution with a bias to the left side. It seems very likely that a peak in the distribution at
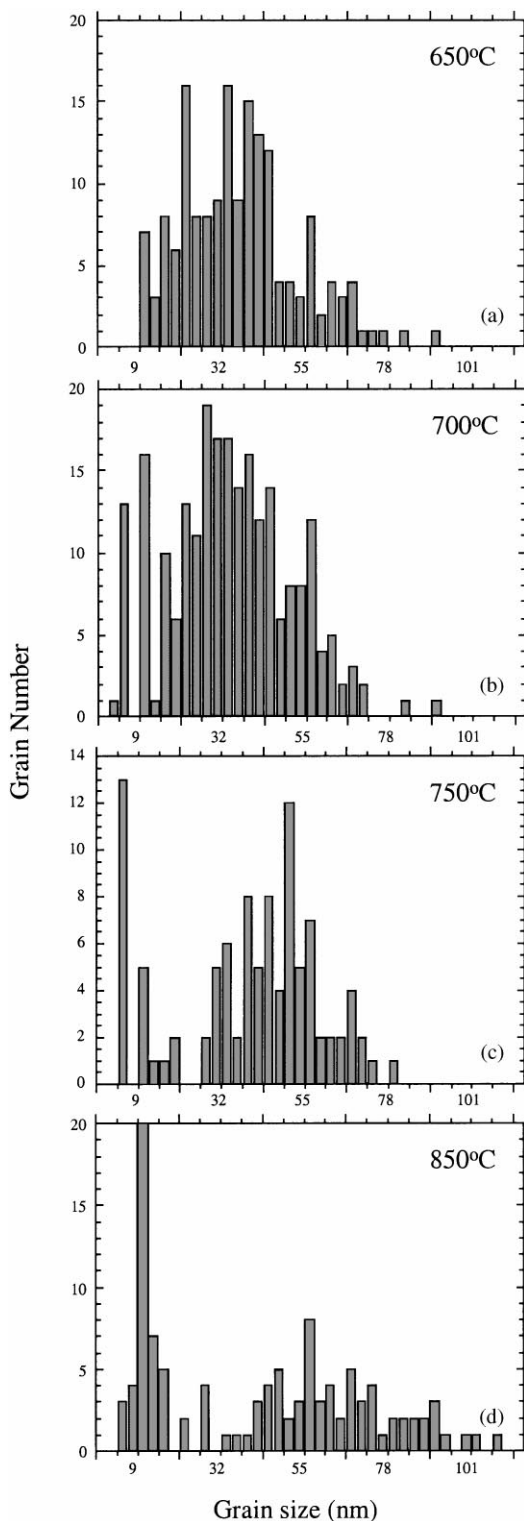
a small grain size exists in the chart. The average value of the grain size of sample B is 40 nm. Fig. 6c clearly exhibits two separate peaks at 5 and 45 nm that belong to the intergranular phase and main phase, respectively. The main phase peak and the secondary phase peak in Fig. 6d shift significantly to the right compared with the distribution in Fig. 6c. The average grain size of the main phase is 68 nm, while the average value of intergranular phase is 12 nm. It should be pointed out that the third type of the grain as mentioned above in Fig. 5b was not counted in the grain size distribution plot of Fig. 6d. That the grain size of $Nd_2(FeCo)_{14}B$ does not increase much until it is annealed at 850°C is most likely due to the intergranular precipitates. Because of a compositional difference with the main 2-14-1 phase, the precipitates may serve as barriers at the grain boundaries to prevent the $Nd_2(FeCo)_{14}B$ grain coarsening.

Fig. 7 displays hysteresis loops and initial curves measured on the four samples. The 650°C loop shows a large step at low field values and another step at higher field values. These steps are caused by a soft magnetic phase (amorphous matrix) and a hard phase ($Nd_2(FeCo)_{14}B$) co-existing in the sample. However, there is no two-phase behavior present in the 700°C data graph. This result may be due to either the disappearance of the amorphous phase or possibly to the presence of exchange coupling between the hard phase and soft phases (if any), e.g., the residual amorphous phase or the crystalline soft phases. The 750 and 850°C curves display a visible continuous decrease in $H_c$. This is due to the fact that the soft phase grains grow larger as it is heat treated at higher temperatures. Moreover, the 850°C curve shows a negligible kink (arrow) at low field. This result can be attributed to the excessive growth of the soft intergranular phase. The initial curves of samples B–D show low susceptibilities compared with sintered magnets [17]. They also show that the susceptibility increases with the annealing temperature. The low initial susceptibility can be interpreted either by the domain wall pinning effect or by single domain behavior. Since the

Fig. 6. Grain size distribution of (a) 650°C, (b) 700°C, (c) 750°C, (d) 850°C samples.
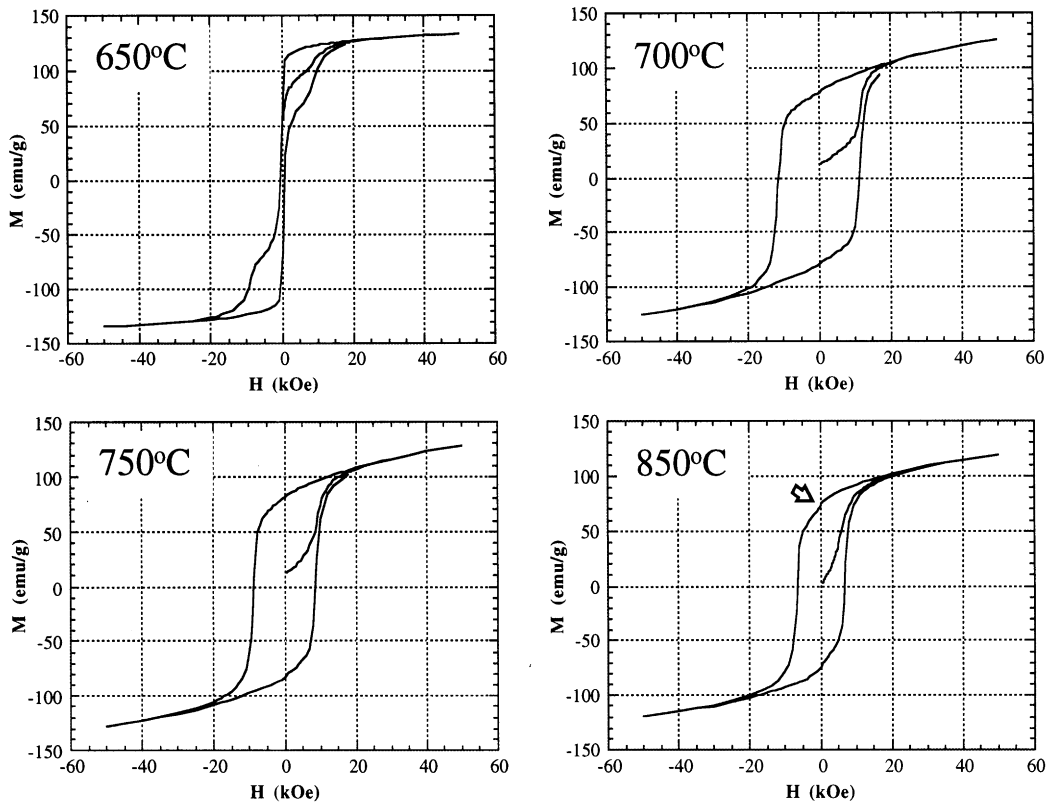
Fig. 7. Hysteresis loops and initial magnetization curves of the four samples.

grain size of all the four samples is much smaller than the critical size of single domain (estimated to be 300 nm for an isolated particle, this value could be greater for grains in a favorable magnetostatic surroundings), the latter interpretation should be responsible for the low susceptibility observed at low field during the first magnetization. Moreover, as the $Nd_2(FeCo)_{14}B$ grains are observed coarse at higher annealing temperatures, the single domain behavior is reduced. As a result, the initial susceptibility increased with the annealing temperature.

## 4. Magnetic domain structure

Generally, there are two ways to image magnetic contrast, Fresnel mode and Foucault mode. In the first mode, when image is off-focused, contrast arises wherever there is a varying component of magnetic induction. Thus magnetic domain walls can be revealed. Inside a Fresnel image a dark region indicates that there is little variation in magnetization direction and that a single domain is observed, while a bright or a gray line implies a domain boundary at the line position. It should be noted that the width of the domain wall increases with the off-focus value of the image. In the Foucault mode the contrast depends on the off-centering of the objective aperture. As a result, domains with component of magnetic induction being 90° or −90° to the displacement of the aperture can be shown as bright or dark regions, respectively.

The Fresnel images (Fig. 8a and Fig. 8b) of sample B show that the domain size varies within the same specimen. The domain size in Fig. 8b is
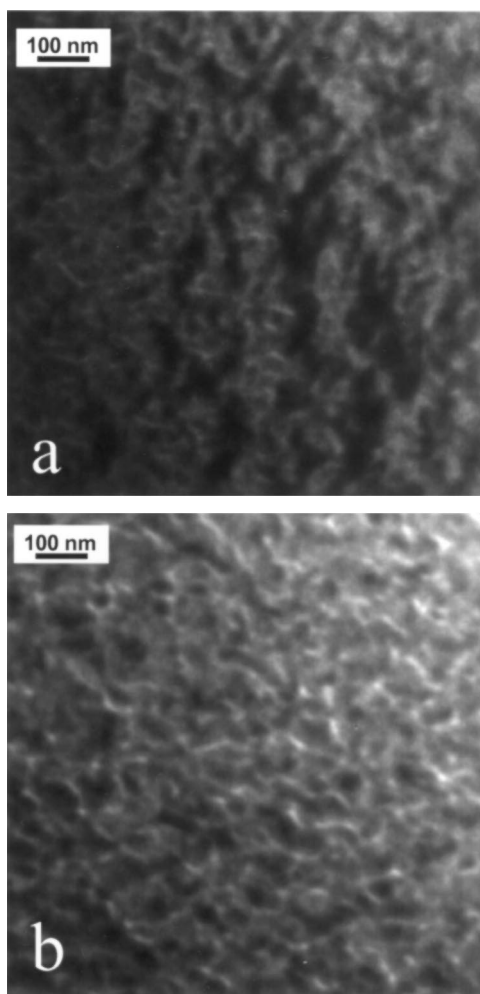
Fig. 8. (a) and (b) Fresnel images of the 700°C sample.

nucleation will not occur inside most of the exchange-coupling domains during the initial magnetization. This result is consistent with the low susceptibility of the initial magnetization curve as mentioned above.

Fig. 9a is a bright field image exhibiting the grain size, which is almost the same as the domain size shown by the Fresnel image in Fig. 9b. This result means that there is little exchange coupling between the grains in this region of the specimen. Fig. 9c and Fig. 9d are two Foucault images of the same region. These two images are obtained with the aperture displaced in opposite directions (black arrows). In Fig. 9c, a snake-shaped black domain can be observed. While in Fig. 9d, the 'snake' becomes white due to the opposite displacement of the aperture. The length of the snake is about 600 nm. Other shorter domains can be seen beside the longest domain. The wavy nature of these domains suggests that a magnetostatic interaction exists between the $Nd_2(FeCo)_{14}B$ grains. Such kind of domains cannot be observed from the Fresnel image in Fig. 9b, which shows magnetic contrast arises at every grain boundary. These results indicate that the magnetization directions of the grains on the 'snake' are not parallel to each other. They are, however, roughly aligned in a zigzag way. Hence, these grains have the same contrast in the Foucault image when the aperture is displaced at the direction perpendicular to the 'snake'. The four particles pointed out by white arrows in Fig. 9b are single domain particles as confirmed by the observation of the domain boundaries around these particles. It is interesting to notice that in Fig. 9c and Fig. 9d only the lower three particles participate in forming the wavy interactive domain, while the top one does not.

## 5. Conclusions

Heat treated melt-spun ribbons of $(Nd_{0.95}La_{0.05})_{9.5}$-$Fe_{bal}Co_5Nb_2B_{10.5}$ have been studied systematically studied by SQUID magnetometry, CTEM and LTEM. Due to the intergranular phases, the grain size of the $Nd_2(FeCo)_{14}B$ does not increase much until annealed at 850°C. Soft magnetic phases in

similar to the grain size, suggesting that the $Nd_2(FeCo)_{14}B$ grains are single-domain particles. The domains in Fig. 8a, on the other hand, generally consist of several grains, which indicates that a strong exchange coupling exists between neighboring grains. In this case, the domain boundaries occur only at the grain boundaries where exchange coupling is weak.

It can be seen in Fig. 8a that most of the exchange-coupled domains are still much smaller than the critical grain size of single domain particles. It is therefore expected that the domain wall
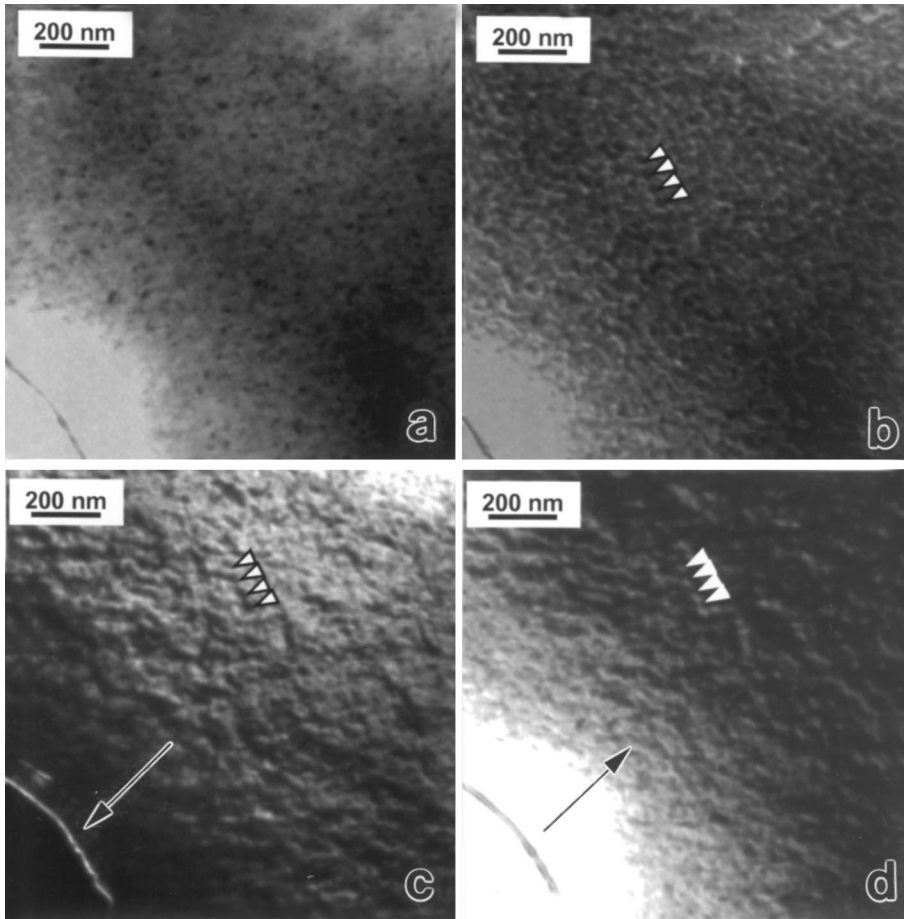
Fig. 9. (a) Bright field image of the 700°C sample, (b) Fresnel image, (c) and (d) Foucault images with opposite aperture displacements indicated by the white arrows.

terms of $Fe_3B$ and $\alpha$-Fe were found precipitating at grain boundaries. The growth of soft magnetic phases with the increase of annealing temperature caused a drop in the coercivity $H_c$ in the samples. When heat treated at 850°C, some of the soft phase grows excessively, thereby weakening the exchange coupling with the $Nd_2(FeCo)_{14}B$ phase. The grains of $Nd_2(FeCo)_{14}B$ are either exchange-coupled or magnetostatically-coupled. Long wavy interactive domains were observed in the regions that are presumably dominated by magnetostatic coupling. The domain size in the region dominated by exchange-coupling is smaller than the critical grain size for a single domain particle. This explains the low susceptibility of the sample during initial magnetization.

## References

[1] J.F. Herbst, J.J. Croat, J. Magn. Magn. Mater. 100 (1991) 57.

[2] Y.B. Kim, W.S. Park, H.T. Kim, Y.S. Cho, C.S. Kim, M.J. Park, T.K. Kim, J. Appl. Phys. 77 (1995) 4133.

[3] J.N. Chapman, L.J. Heyderman, S. Yong, D.M. Donnet, P.Z. Zhang, H.A. Davis, Scripta Metall. Mater. 33 (1995) 1807.

[4] M. Seeger, J. Bauer, G. Rieger, H. Kronmüller, J. Bernardi, J. Fidler, J. Magn. Magn. Mater. 140–144 (1995) 1059.

[5] W.C. Chang, S.H. Wu, B.M. Ma, C.O. Bounds, J. Magn. Magn. Mater. 167 (1997) 65.

[6] J. Bauer, M. Seeger, A. Zem, H. Kronmüller, J. Appl. Phys. 80 (1996) 1667.

[7] H. Kronmüller, K.-D. Durst, M. Sagawa, J. Magn. Magn. Mater. 74 (1988) 29.

[8] M. Grönefeld, H. Kronmüller, J. Magn. Magn. Mater. 88 (1990) L267.

[9] M. Sagawa, S. Hirosawa, J. Mater. Res. 3 (1988) 45.

[10] D. Givord, P. Tenaud, T. Viadieu, IEEE Trans. Magn. Mag. 24 (1988) 1921.

[11] R. Fischer, H. Kronmüller, Phys. Rev. B 54 (1996) 7284.

[12] R. Coehoorn, D.B. de Mooji, J.P.W.B. Duchatean, K.H.J. Buschow, J. Phys. (Paris) 49 (1988) C8–669.

[13] A. Manaf, R.A. Buckley, H.A. Davis, J. Magn. Magn. Mater. 128 (1993) 302.

[14] A. Manaf, M. Ai-Khafaji, P.Z. Zhang, H.A. Davis, R.A. Buckley, W.M. Rainforth, J. Magn. Magn. Mater. 128 (1993) 307.

[15] W.C. Chang, S.H. Wu, B.M. Ma, C.O. Bounds, S.Y. Yao, J. Appl. Phys. 83 (1997) 2147.

[16] J.N. Chapman, J. Phys. D 17 (1984) 623.

[17] M. Seeger, J. Bauer, H. Kronmüller, J. Bernardi, J. Fidler, J. Magn. Magn. Mater. 138 (1994) 294.